Science Advances

AAAS

Supplementary Materials for

Evidence for a strain-tuned topological phase transition in ZrTe$_5$

Joshua Mutch, Wei-Chih Chen, Preston Went, Tiema Qian, Ilham Zaky Wilson, Anton Andreev,
Cheng-Chien Chen*, Jiun-Haw Chu*

*Corresponding author. Email: jhchu@uw.edu (J.-H.C.); chencc@uab.edu (C.-C.C.)
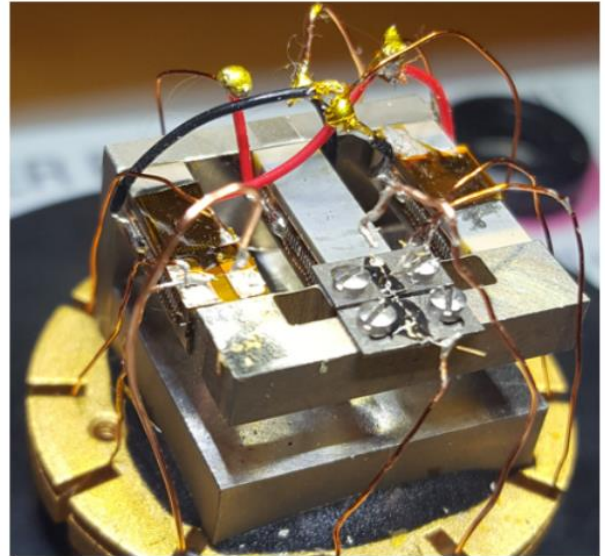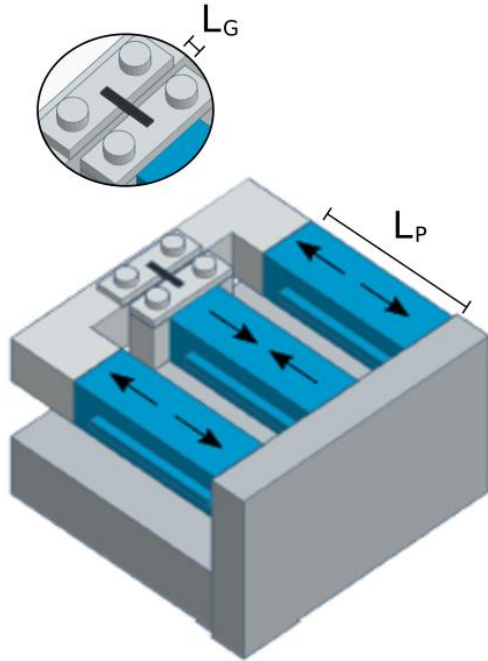
This PDF file includes:

Fig. S1. Schematic and picture of piezo device. By applying inducing strain in the outer and middle actuators (blue), stress can be applied to a crystal glued across the gap (black). The displacement of the gap is a factor of of $2L_P/L_G$ larger than the strain of any single piezostack. Photo Credit: Joshua Mutch, University of Washington.
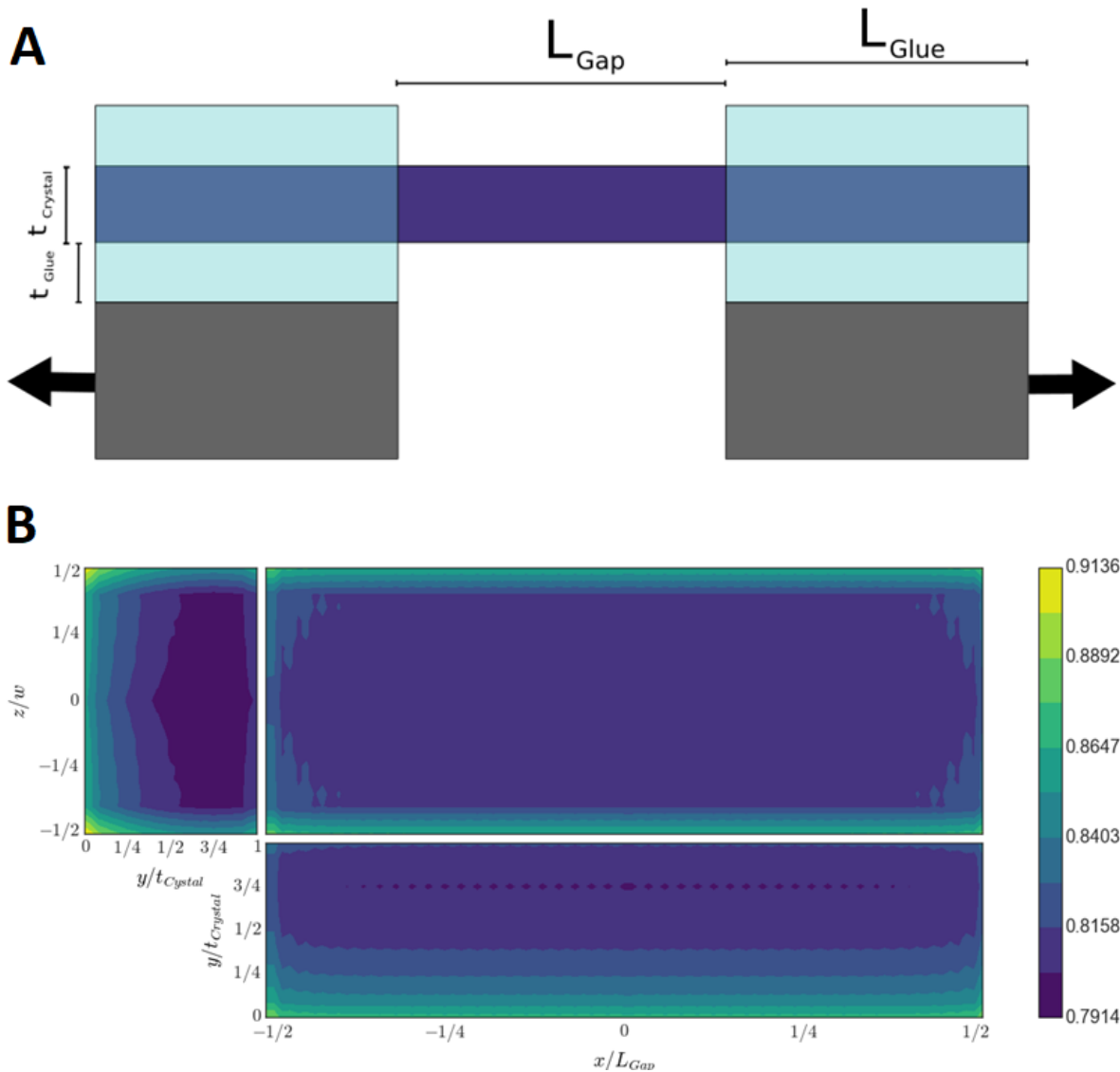
Fig. S2. Finite element analysis of strain transmission. (**A**) Schematic of system modelled by finite element analysis. For our analysis, we assumed $t_{Glue}/t_{Crystal}=0.5$ and $L_{Glue}/L_{Gap}=1$, reasonable assumptions given optical images of the experiment. (**B**) Strain transmission α averaged through the length (upper left), thickness (upper right), and width (bottom right) of the crystal, modelled after a crystal with dimensions of Growth 1, Sample 2.

Fig. S3. Sample aging and zero-strain tuning. (**A** & **B**) Resistance versus temperature for two different ZrTe$_5$ crystals, measured 18 days apart. The sample wa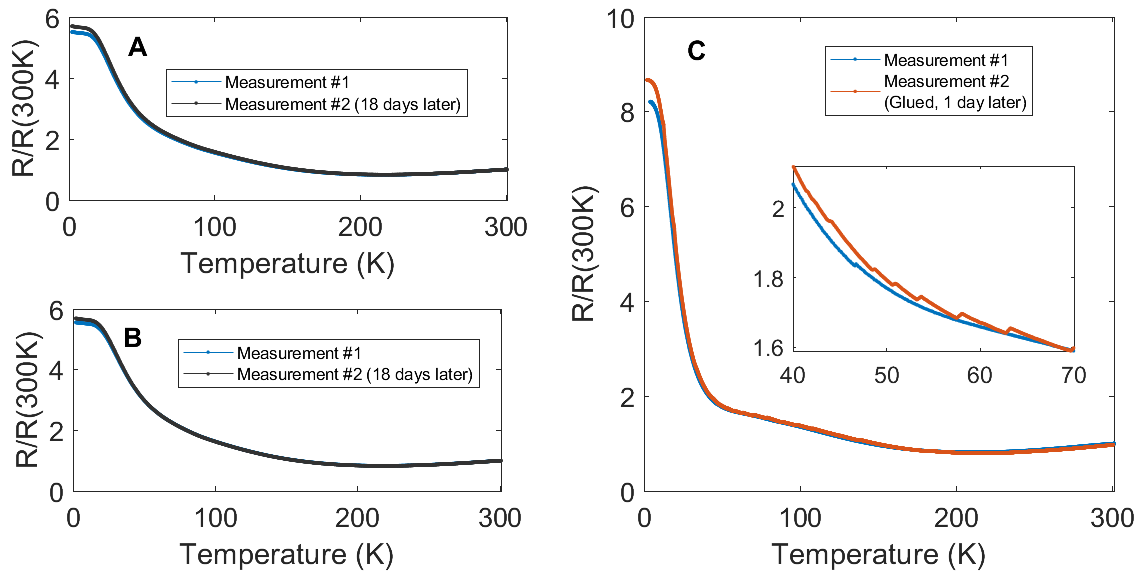s stored in atmosphere during the 18 days between measurements. The 2K resistance increased by 3.4% (crystal shown in panel A) and 2.4% (panel B) between measurements. (**C**) A third crystal was glued to a strain mechanism one day after its unstrained resistance was measured. The resistance was monitored as the crystal was cooled, and the strain was adjusted to tune the resistance to the unstrained calibration resistance. However, at low temperatures, the ability to tune the resistance to the calibration data was lost. At 2K, the minimum resistance (R_{min}) of the strained crystal was 5.4% higher than the resistance of the unstrained state.
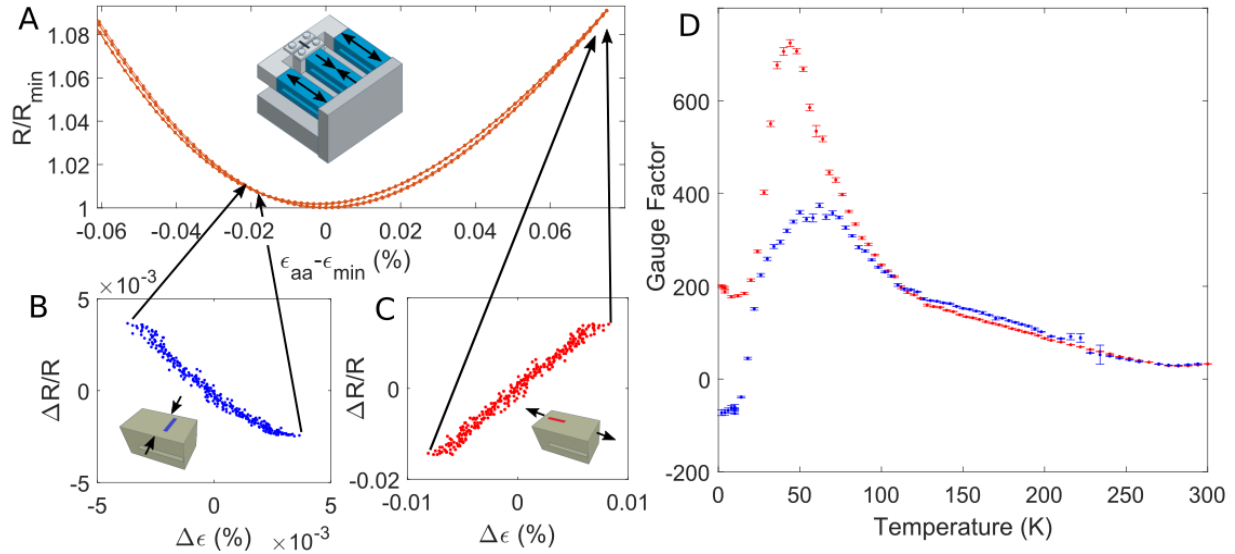
Fig. S4. Comparison between three-piezo and single-piezo elastoresistivity measurement.
(**A**) Resistance versus strain at 2K for sample S2 mounted on the 3-piezo mechanism. (**B & C**) Resistance versus strain at 2K for samples glued directly to the surface of a piezostack, glued perpendicular (B) and parallel (C) to the polling direction of the piezostack. (**D**) Gauge factor, defined as the linear slope of resistance as a function of strain, for the two crystals glued perpendicular and parallel the piezo polling direction. Below 100K, the GF becomes sensitive to the sample mounting method.
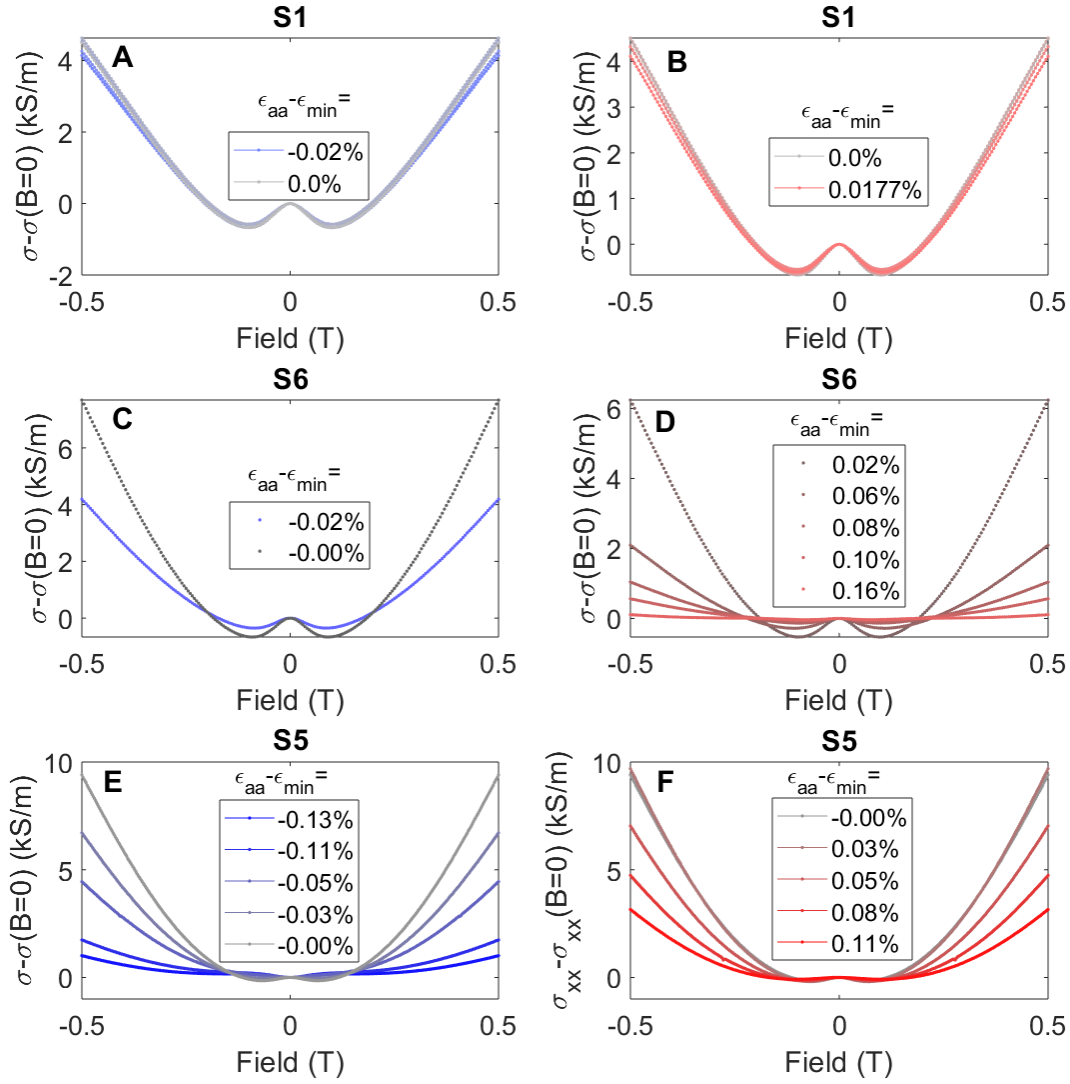
Fig. S5. Additional longitudinal magneto-transport measurement as a function of strain. Positive magnetoconductance for compressive (**A**, **C**, & **E**) and tensile (**B**, **D** & **F**) strains with respect to ϵ_{min}. The strength of the positive magnetoconductance is suppressed for strains away from the ϵ_{min}. Panels (**A** & **B**), (**C** & **D**), and (**E** & **F**) correspond to measurements on three different crystals, S1, S6, and S5, respectively. Panels E & F correspond to the same crystal for which high field data is presented in Fig. 3 of the main text.
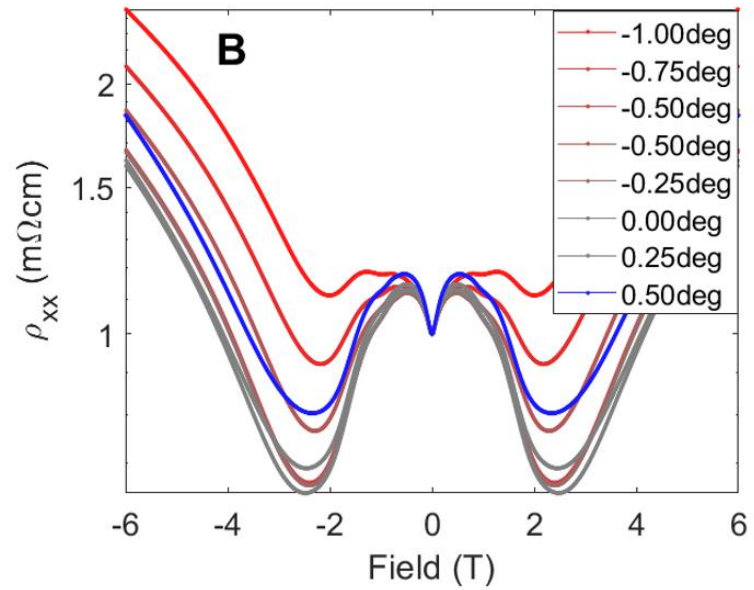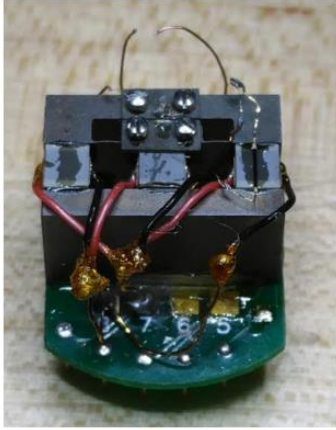
Fig. S6. Angle dependence of longitudinal magnetoresistance. (**A**) Rotating apparatus puck. A smaller version of our strain apparatus was constructed to fit on a Quantum Design Dynacool rotation puck. Photo Credit: Joshua Mutch, University of Washington. (**B**) Magnetoresistance for magnetic fields slightly misaligned to the direction of the current. For the best alignment, the negative longitudinal magnetoresistance is strongest. As the misalignment is increased, the negative longitudinal magnetoresistance is suppressed, and eventually destroyed for 1-degree misalignment.

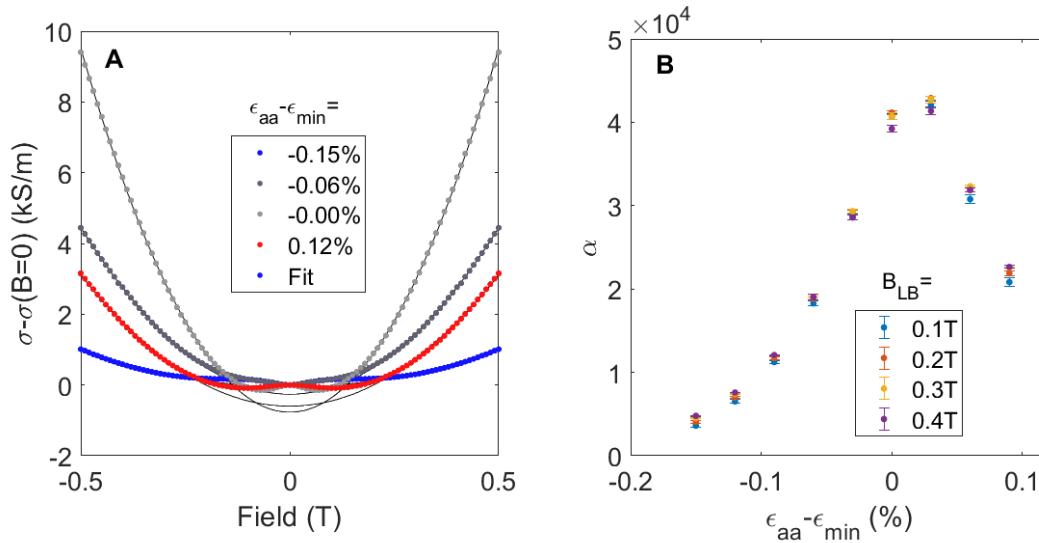**Fig. S7. Fitting of positive longitudinal magnetoconductance.** (**A**) Positive magnetoconductance for several strain setpoints close to ϵ_{min}. For very low fields (B<0.1T), a small negative magnetoconductance is observed, followed by a positive magnetoconductance for higher fields. The conductance is fitted to the equation $\sigma(B) = \sigma_0 + \alpha B^2$, where α is a positive coefficient proportional to the helicity relaxation time. To eliminate errors to the fit associated with the small dip of magnetoconductance near zero field, the data was fitted only for the magnetic field bounded between a lower bound and 0.5T, $B_{LB} < |B| < 0.5T$. The black fit lines shown in (A) are for $B_{LB} = 0.2T$. (**B**) The coefficient α as a function of strain. α is plotted for several choices of B_{LB}, and the choice of B_{LB} is found to not significantly influence the fitting of α. For the data shown in Fig. 3C of the main text, $B_{LB} = 0.2T$.
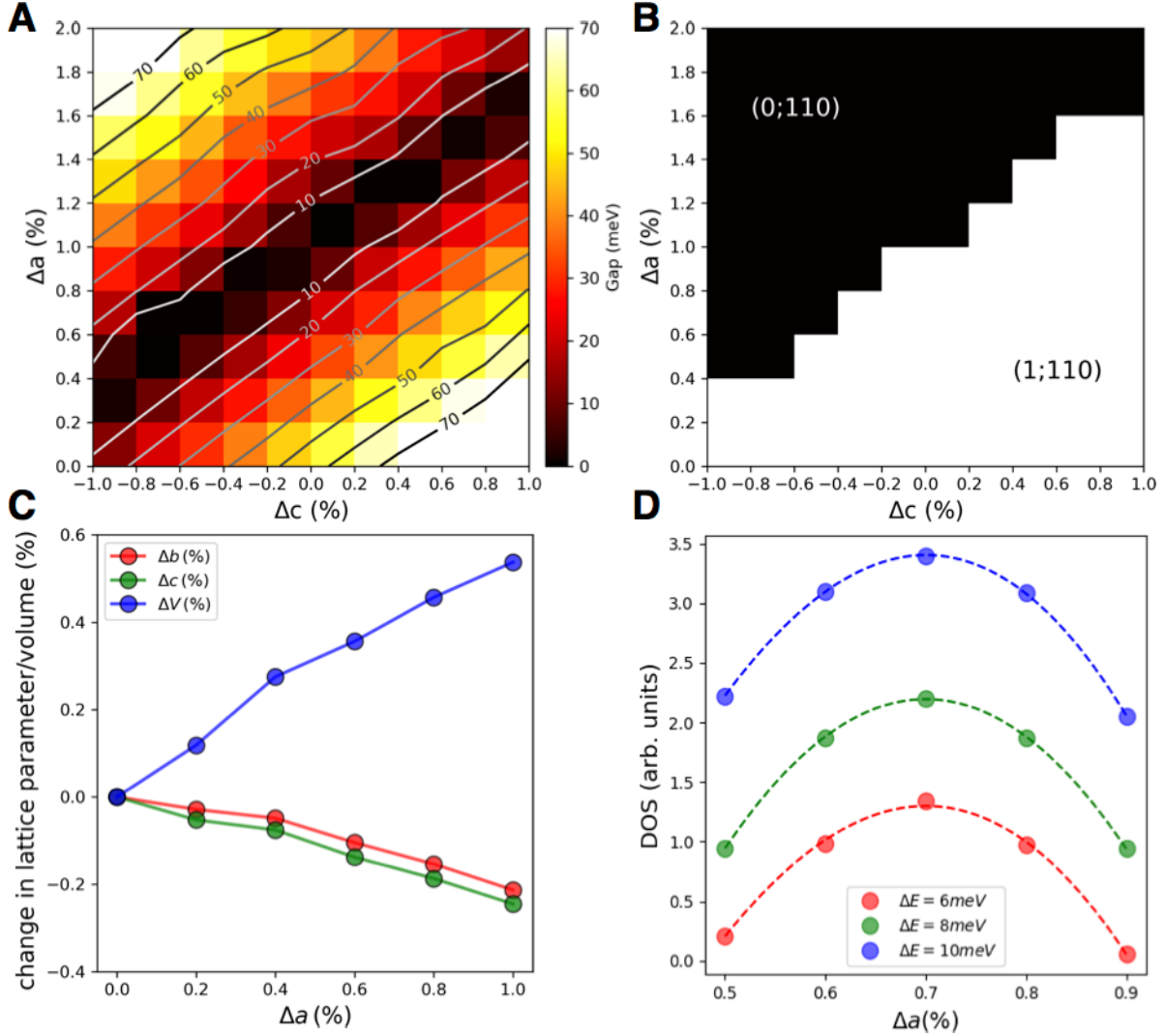
Fig. S8. DFT calculations of Z_2 topological indices, Poisson ratio, and DOS. (**A**) Zone-center energy gap computed by DFT as functions of variations in the lattice a and c parameters. The change of the b-lattice constant has a much weaker effect on the bandgap, the inclusion of which makes no qualitative change to the argument. (**B**) Topological phase diagram and Z_2 indices for different strained structures. Phase transition between the STI (1;110) and WTI (0;110) states is directly controlled by closing the zone-center energy gap. (**C**) Changes in the b/c lattice parameters and volume as a function of strain in the a-direction; the fully relaxed structure calculations were performed with the van der Walls density functional theory (vdW-DFT). (**D**) Strain dependence of density of states (DOS) around the Γ point. The DOS was calculated by making a k-grid of 21 x 21 x 11 points around the Γ point ($\pm 0.01\ b_1$, $\pm 0.01\ b_2$, $\pm 0.01\ b_3$) and counting the states within $E_{fermi} \pm \Delta$, where Δ ranges from 6 to 10 meV (corresponding to 70 to 120 K).
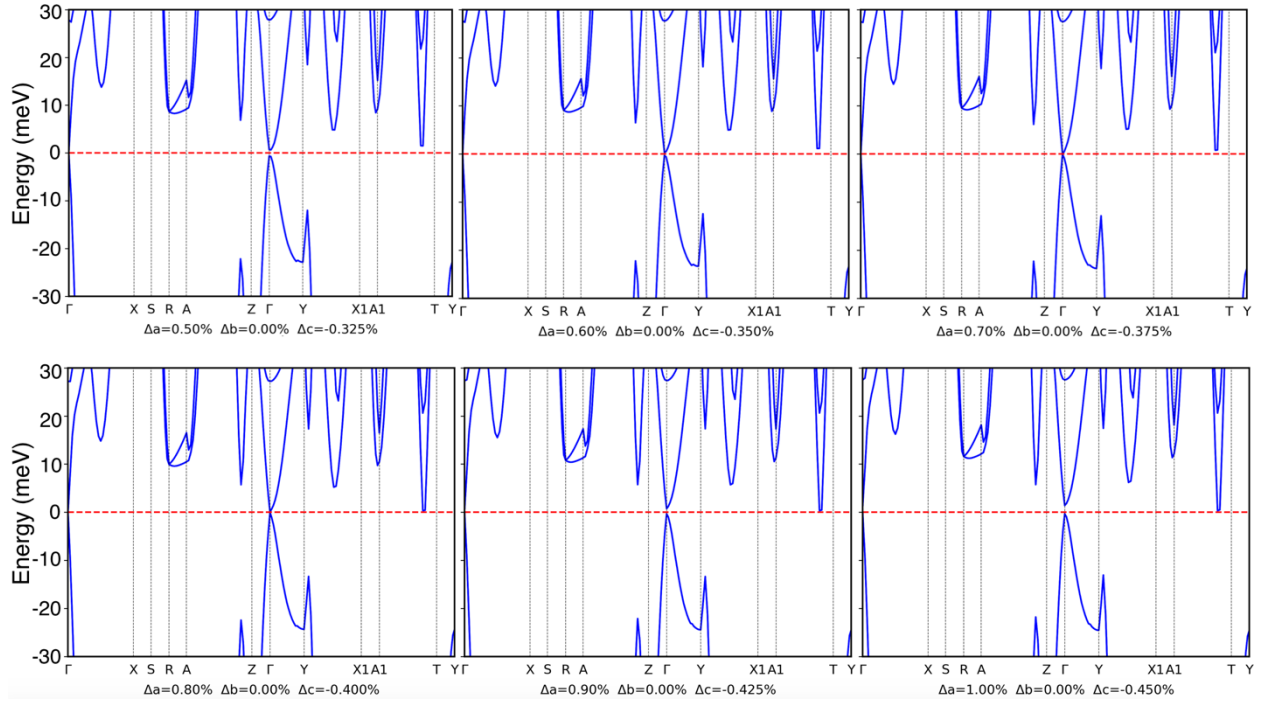
Fig. S9. DFT band structures for ZrTe₅ in different strained states. The horizontal red dashed line indicates the Fermi level. The labeling of the high-symmetry k-points is based on the Brillouin zone of the primitive unit cell.

Sample	Growth	$(L_G{:}w{:}t)$ (µm)	α	Q(2K)	n (10^{15}cm^{-3})
S1	1	962:60:10	0.93	4.9×10^5	0.6
S2	1	1,060:120:40	0.81	2.1×10^5	2.4
S3	1	490:21:15	0.89	2.7×10^5	1.6
S4	2	800:40:60	0.82	7.8×10^5	0.3
S5	1	0.77:0.03:0.02	0.90	4.1×10^5	0.8
S6	1	0.5:0.021:0.015	0.89	-	-

Table S1. Dimensions, 2 K resistivity, and QC of each sample crystal. The average strain relaxation α is calculated from these parameters by finite element analysis. The deformation in the vertical axis, Δy, is also calculated. The quadratic response to strain is denoted as Q. The carrier density n calculated from Q(2K) is numerically computed from a Boltzmann transport equation of the Dirac dispersion.